LETTER

doi:10.1038/nature10430

Mechanical strain in actin networks regulates FilGAP and integrin binding to filamin A

A. J. Ehrlicher[1,2], F. Nakamura[1], J. H. Hartwig[1], D. A. Weitz[2] & T. P. Stossel[1]

Mechanical stresses elicit cellular reactions mediated by chemical signals. Defective responses to forces underlie human medical disorders[1–4] such as cardiac failure[5] and pulmonary injury[6]. The actin cytoskeleton's connectivity enables it to transmit forces rapidly over large distances[7], implicating it in these physiological and pathological responses. Despite detailed knowledge of the cytoskeletal structure, the specific molecular switches that convert mechanical stimuli into chemical signals have remained elusive. Here we identify the actin-binding protein filamin A (FLNA)[8,9] as a central mechanotransduction element of the cytoskeleton. We reconstituted a minimal system consisting of actin filaments, FLNA and two FLNA-binding partners: the cytoplasmic tail of β-integrin, and FilGAP. Integrins form an essential mechanical linkage between extracellular and intracellular environments, with β-integrin tails connecting to the actin cytoskeleton by binding directly to filamin[4]. FilGAP is an FLNA-binding GTPase-activating protein specific for RAC, which *in vivo* regulates cell spreading and bleb formation[10]. Using fluorescence loss after photoconversion, a novel, high-speed alternative to fluorescence recovery after photobleaching[11], we demonstrate that both externally imposed bulk shear and myosin-II-driven forces differentially regulate the binding of these partners to FLNA. Consistent with structural predictions, strain increases β-integrin binding to FLNA, whereas it causes FilGAP to dissociate from FLNA, providing a direct and specific molecular basis for cellular mechanotransduction. These results identify a molecular mechanotransduction element within the actin cytoskeleton, revealing that mechanical strain of key proteins regulates the binding of signalling molecules.

The composite cytoskeleton network *in vivo* provides dynamic cellular structure and actively generates movement. A physiological reconstituted *in vitro* network of actin and FLNA creates an elastic gel mechanically dominated by the rod-like actin filaments and cross-linked by flexible FLNA molecules. Applying strain to this network readily deforms FLNA crosslinks (Fig. 1a, b), and the specific structure and actin binding of FLNA suggest how these deformations might affect FLNA's interaction of with some of its 90 or so other currently identified binding partners[9].

FLNA is an extended homodimer composed of two identical subunits, each having an amino-terminal actin-binding domain followed by 24 immunoglobulin repeats[12] (Fig. 1c, d). The actin-binding domains and repeats 1–15 are designated 'rod 1' and form a linear structure that binds actin filaments. Repeats 16–23, comprising 'rod 2', however, form compact globular clusters that do not interact with actin filaments and contain most of FLNA's binding-partner sites. Strain-dependent reversible straightening of these domains contributes to FLNA–actin network flexibility and may regulate local binding-partner affinity (Supplementary Fig. 1). Here we examine the effects of mechanical strain on FLNA's interactions with two key rod-2 binding partners; cytoplasmic β-tail integrin, which nucleates an extensively characterized signalling[13] and adhesion[14] complex, and FilGAP, which is a GTPase specific for RAC, a regulator of cellular activity such as actin assembly[10]. Mechanical strain may regulate partner binding, and we propose that stretching FLNA crosslinks not only causes FilGAP to unbind, but also causes integrin to bind more strongly (Fig. 1c, d and Supplementary Fig. 1). Neighbouring immunoglobulin repeats cover integrin binding sites on FLNA repeats 19 and 21 (refs 15, 16), but computational simulations suggest that rod 2 of FLNA is highly flexible and that physiological forces are sufficient to expose these cryptic sites, allowing integrin to bind[17,18] (Supplementary Fig 1a, b). FilGAP binding occurs on each repeat 23, suggesting that FilGAP is able to bind repeat 23 on both subunits simultaneously when unstressed, providing sufficient avidity to promote FilGAP association with FLNA (Fig. 1c and Supplementary Fig. 1c). Mechanical stretching of FLNA spatially separates repeats 23, preventing FilGAP from binding simultaneously to both[19], thus causing it to dissociate (Fig. 1d and Supplementary Fig. 1d).

To test these hypotheses and measure the effect of mechanical stress on binding-partner interactions with FLNA, we reconstituted networks of polymerized actin (F-actin) and FLNA containing the binding-partner FilGAP or β_7-integrin. To quantify the strain-dependent

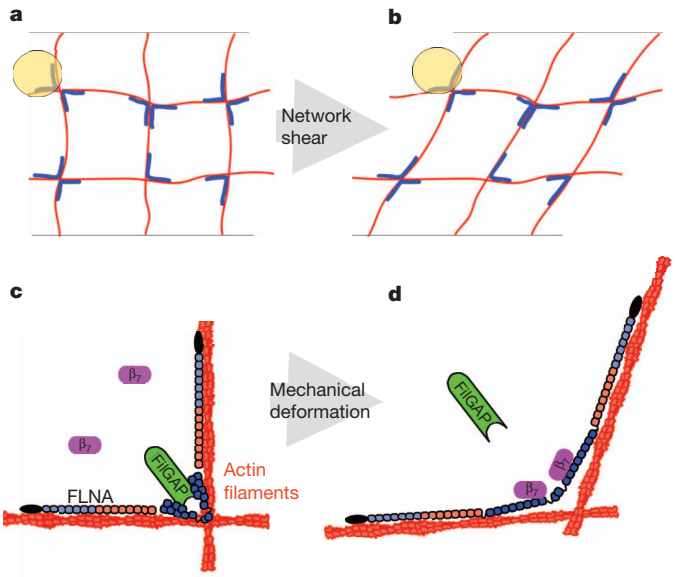

Figure 1 | Differential mechanotransduction in FLNA occurs through spatial separation of binding sites and opening cryptic sites. **a**, A gel of actin (red) crosslinked with filamin (blue) forms an orthogonal network. **b**, When this network is strained, crosslinks are deformed. **c**, The actin-binding domain of FLNA is shown in black, and is followed by repeats 1–7 (light blue) and 8–15 (red/orange), which form the linear rod-1 region. Repeats 16–23 (dark blue) form the compact rod-2 region. FilGAP (green) binds repeats 23 and the cytoplasmic domain of β_7-integrin (purple) is unbound. **d**, When FLNA is mechanically deformed, the cryptic integrin site on repeat 21 is exposed allowing β_7-integrin to bind, whereas repeats 23 are spatially separated, preventing FilGAP from binding them both.

[1]Translational Medicine Division, Department of Medicine, Brigham and Women's Hospital, Harvard Medical School, Boston, Massachusetts 02115, USA. [2]School of Engineering and Applied Sciences, Department of Physics, Harvard University, Cambridge, Massachusetts 02138, USA.

kinetics of these partners of FLNA, we developed fluorescence loss after photoconversion (FLAC), which takes advantage of the rapid photoactivation or conversion of photoactivatable fluorescent proteins (PAFPs) as a high-speed analogue to fluorescence recovery after photobleaching[11]. In FLAC, a sample with an initially non-fluorescent binding partner is locally illuminated with a 50-ms pulse of 405-nm light, rapidly and permanently activating PAFP-conjugated partner fluorescence (Supplementary Figs 4 and 5). Photoactivation fluorescently marks the sample faster than conventional photobleaching, and without the requirement of high excitation flux. After activation, unbound PAFP rapidly diffuses away, decreasing the fluorescence signal, whereas bound PAFP dissociates more slowly. The time-dependent decay of PAFP intensity reveals the kinetics of the FLNA binding partner, as slower decay indicates slower unbinding, and thus provides a direct, high-speed assay of dissociation.

We tested the utility of these PAFP constructs in assaying binding kinetics by reconstituting F-actin and the PAFP-labelled binding partner with different forms of FLNA that have higher or lower affinities for β_7-integrin or FilGAP. Consistent with immunoprecipitation data (Supplementary Fig. 3b, c), the fluorescence decay of β_7-integrin labelled with photoactivatable green fluorescent protein (PA-GFP β_7-integrin) was faster in wild-type FLNA networks than in the del41 variant (Supplementary Movie 1), demonstrating relatively stronger binding in the del41 mutant than in wild type. The fluorescence decay of PA-GFP FilGAP was slower in wild-type FLNA networks than in the M2474E mutant (Supplementary Movie 2), also in agreement with immunoprecipitation data (Supplementary Fig. 3a).

We then applied the FLAC methodology to measure the mechanosensitive aspect of interactions between PAFP-labelled binding partners and FLNA. We sheared networks of F-actin and FLNA containing PAFP-tagged FilGAP or β_7-integrin in a precise and highly controlled fashion using a microscope stage comprising a stationary coverslip for the bottom of the sample and a piezo-controlled linear actuator for the top. When the FLNA/F-actin network was not strained, β_7-integrin had a characteristic exponential decay time of 1.3 ± 0.1 s. The application of a shear strain, $\gamma = 0.28$, increased this time to 3.5 ± 0.3 s (Fig. 2a). The change in fluorescence decay rate under strain describes how the geometric state of FLNA affects dissociation of β_7-integrin; thus, mechanically stretching FLNA molecules enhanced the β_7-integrin binding. By contrast, FilGAP behaved qualitatively oppositely: unstrained networks had a characteristic fluorescence decay time of 3.6 ± 0.7 s, which decreased to 0.6 ± 0.1 s when a shear strain of $\gamma = 0.28$ was applied (Fig. 2b). FLNA does not permanently crosslink actin, and by unbinding and rebinding on the timescale of ~6 min (Supplementary Fig. 6), it dynamically allows the network to relax to an unstressed state. After 10 min under strain, the network had sufficient time to dissipate internal stress through FLNA remodelling, and the fluorescence decay time increased to 6.1 ± 0.7 s, demonstrating the reversibility of strain-modulated FilGAP binding to FLNA (Fig. 2b).

The application of unidirectional shear reveals the effects of strain on partner binding to FLNA; however, cells commonly generate internal stresses using molecular motors such as myosin. To examine the effects of cytoskeleton-induced stress, and as a physiological technique complementary to external shear, we included myosin II in the networks to generate contractile stress[20] (Supplementary Fig. 9 and Supplementary Movie 3). We allowed the composite network to assemble and come to an unstressed equilibrium state over ~6 h, after which time the incorporated myosin II had ceased contracting, by enzymatically exhausting the pool of added ATP, and dynamic FLNA remodelling had dissipated internal stresses. For unstressed FLNA, we measured β_7-integrin and FilGAP fluorescence decay times of 1.6 ± 0.1 and 1.5 ± 0.1 s, respectively (Fig. 3a, c). Including photolabile 'caged' ATP in the sample allowed us to release fresh ATP and restart myosin motor activity[21,22], which contracts the actin network and strains FLNA crosslinks. In myosin-stressed FLNA, the integrin unbinding time increased to 2.5 ± 0.2 s but the FilGAP unbinding time decreased to 0.9 ± 0.1 s (Fig. 3b, d). The application of either external shear or myosin contraction resulted in increased integrin binding and decreased FilGAP binding, demonstrating the robust, opposite behaviours of these FLNA binding partners.

The FLNA-crosslinked actin cytoskeleton is a large, percolated network that, owing to its filamentous actin structure, can readily transmit large mechanical deformations over long intracellular distances, yet FLNA is mechanosensitive to nanometre-scale molecular deformations. This range of length scales contrasts with that of focal adhesion mechanosensitivity, which detects local mechanics and is limited to small spatial and strain scales owing to their size and connectivity[23,24].

In conclusion, we have developed *in vitro* systems to study quantitatively protein–protein interactions under mechanical force. Using PAFPs with the FLAC technique provides the increases in time resolution necessary for measuring transient kinetics, without the harsh intensity or duration of bleaching exposure required for fluorescence recovery after photobleaching. The results presented here establish FLNA as a mechanotransductive substrate within the cytoskeleton and highlight the utility of *in vitro* systems, in combination with FLAC, to determine quantitative responses of specific proteins.

Mechanotransduction *in vitro* provides the biological specificity necessary for understanding how these complex regulatory signals may operate *in vivo*. Cellular mechanotransduction has been shown to induce rapid biochemical activity over long distances[25]. Because mechanical stimuli induce relatively large local deformations that decrease in magnitude with distance from the site of application,

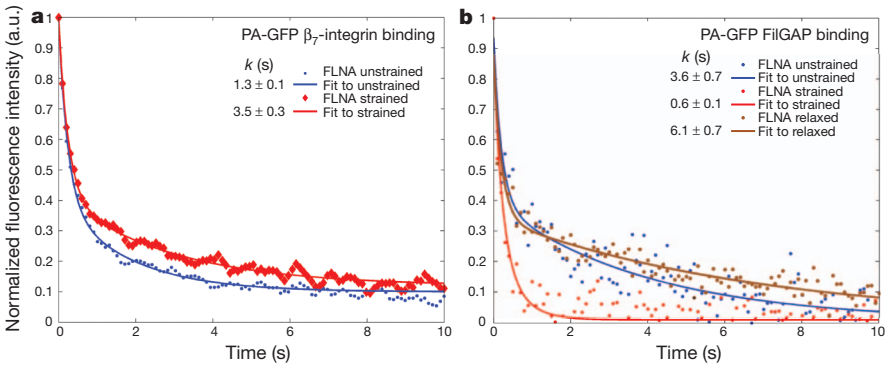

Figure 2 | External bulk shear of F-actin/FLNA networks alters FLNA's binding affinity for β_7-integrin and FilGAP. a, Fluorescence intensity of PA-GFP β_7-integrin as a function of time after photoactivation. When unstrained (blue), fluorescence of β_7-integrin decays with a characteristic time constant of $k = 1.3$ s. Following the application of a shear strain of $\gamma = 0.28$, the time constant increases to 3.5 s, as the integrin dissociates more slowly from FLNA ($n = 18$). a.u., arbitrary units. **b**, Fluorescence intensity of PA-GFP FilGAP as a function of time after photoactivation. Unstrained (blue) FilGAP's fluorescence decay time is $k = 3.6$ s. A shear strain of $\gamma = 0.28$ (red) decreased k to 0.6 s. This behaviour is reversible, and after allowing the network to relax for 10 min, removing all strain, k increases to 6.1 s (brown) ($n = 10$).

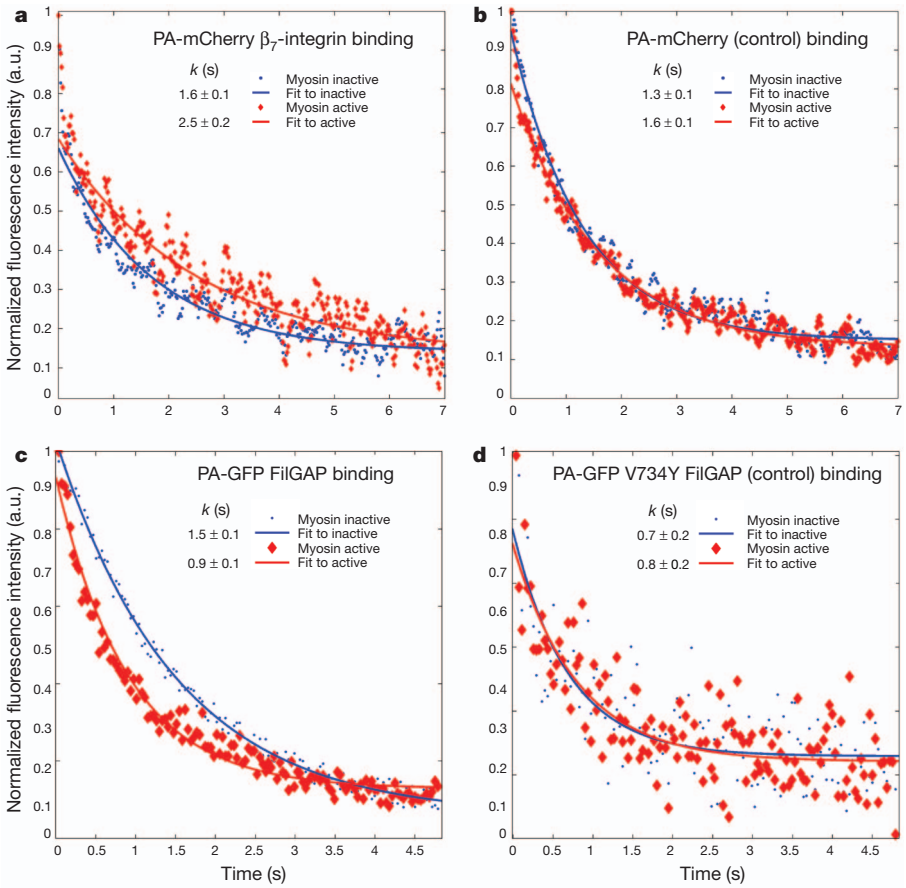

Figure 3 | Myosin II forces applied to F-actin/FLNA networks change FLNA's binding affinity to β_7-integrin and FilGAP. **a**, When depleted of ATP, myosin is in a rigor state. The FLNA within the network is not stressed and PA-GFP β_7-integrin fluorescence decays with a characteristic time constant of $k = 1.6$ s (blue). After caged ATP is released, myosin reactivates, straining FLNA crosslinks. The decay time constant increases to 2.5 s because the integrin dissociates more slowly from FLNA under stress. **b**, PA-mCherry alone as a control shows no significant difference between the unstrained and strained states. **c**, Fluorescence intensity of PA-GFP FilGAP as a function of time after photoactivation. **d**, In the ATP-depleted state, FilGAP's fluorescence decay time is $k = 1.5$ s, and after release of the caged ATP (red), k decreases to 0.9 s. In PA-GFP V734Y FilGAP, a non-FLNA binding mutant used as a control, the decay time in the unstrained state (0.7 s) is not significantly different from that in the strained state (0.8 s) ($n = 20$).

FLNA mechanotransduction *in vivo* probably provides a rapid, distance-sensitive biphasic response by binding or unbinding integrins or FilGAP, respectively, as a result of the transmitted strain. Physiologically, the localization and binding of these proteins determine their activity. Strain-induced binding of integrin to FLNA may compete with talin binding to integrin[26], thus providing a mechanosensitive switch for integrin activation and adhesion. FLNA's homodimer structure may induce clustering of integrin, thereby reinforcing adhesion and concentrating signalling molecules at a specific location. FilGAP, when unbound from FLNA, relocates to the plasma membrane, where it inactivates RAC[10]. Active RAC levels profoundly affect cell movement[27], and increased RAC activity in FLNA-deficient cells correlates with increased apoptosis[28]. Moreover, our measurements are consistent with *in vivo* studies demonstrating that RAC activity and expression seem to be force-regulated by FilGAP–FLNA interactions, because inhibiting FLNA or FilGAP increases RAC activity but applying local forces to wild-type cells causes FilGAP to decrease RAC activity[28]. Because FLNA does not change FilGAP's catalytic activity, mechanically induced redistribution alone might explain its regulation *in vivo*. Force-dependent conformational changes in structure required for mechanical regulation have been observed in many proteins, including FLNA *in vivo*[29,30]. By identifying FLNA as a mechanosensitive element within the cytoskeleton, we have clarified how RAC and integrin activity may be regulated by a specific molecular mechanotransduction pathway. Identifying mechanotransduction elements may direct novel, targeted therapeutic approaches by correcting or modulating mechanosensitive binding.

METHODS SUMMARY

PAFP fluorophore synthesis. PAFP fluorophore was genetically tagged to binding partners, creating PAFP-labelled β_7-integrin and FilGAP. Solubility and correct binding of labelled partners was confirmed using western blots (Supplementary Fig. 3).

FLAC methodology. An external 405-nm laser was coupled into a Leica SP5 confocal microscope and used to illuminate a central, ~2-μm spot for 50 ms, converting the PAFP from its dark state to its fluorescent state (Supplementary Figs 4 and 5). The decay in the fluorescence intensity, $I(t)$, of the activated fluorophores was monitored and fitted with the exponential $I(t) = ae^{-t/k} + c$, where k is the time constant of characteristic dissociation. Given k values represent best fits plus 95% confidence intervals. In the case of single-step uniaxial strain presented in Fig. 2, data were fitted to $I(t) = ae^{-t/k} + 0.5e^{-t/(0.15s)} + c$ to provide a more accurate fit and compensate for the rapid diffusion of free fluorophore.

Sample cell composition. Shear cell samples consisted of 24 μM actin, 0.12 μM FLNA, ×1 F-actin polymerization buffer (Methods), 2 μM Alexa 546 phalloidin and either PA-GFP FilGAP or PA-GFP β_7-integrin, and were sheared in a piezo-driven shear cell (Supplementary Information). Sheared FLAC measurements for strained networks were acquired approximately 5–10 s after shear. Myosin samples included 24 μM actin, 0.12 μM FLNA, 1 μM myosin II, ×1 activity buffer (Methods) and 2 μM caged ATP, along with 2 μM Alexa 546 phalloidin and PA-GFP FilGAP or 2 μM Alexa 488 phalloidin and PA-mCherry β_7-integrin. Samples were allowed to polymerize and consume available ATP over ~6 h. FLAC measurements were then performed on the ATP-free unstressed network. Subsequently, the caged ATP (Sigma) was released by a 4-s exposure to a diffuse 50-mW, 365-nm light-emitting diode (Prizmatix), and within 3 s the network could be seen to homogenize under myosin contraction (Supplementary Fig. 9 and Supplementary Movie 3). FLAC measurements were then repeated in this active myosin-stressed network to quantify the strain-dependent binding activity.

Full Methods and any associated references are available in the online version of the paper at www.nature.com/nature.

Received 12 April; accepted 5 August 2011.
Published online 18 September 2011.

1. Ingber, D. E. Mechanobiology and diseases of mechanotransduction. *Ann. Med.* **35,** 564–577 (2003).
2. Discher, D. E., Janmey, P. & Wang, Y. L. Tissue cells feel and respond to the stiffness of their substrate. *Science* **310,** 1139–1143 (2005).
3. Moore, S. W., Roca-Cusachs, P. & Sheetz, M. P. Stretchy proteins on stretchy substrates: the important elements of integrin-mediated rigidity sensing. *Dev. Cell* **19,** 194–206 (2010).
4. Hoffman, B. D. *et al.* Dynamic molecular processes mediate cellular mechanotransduction. *Nature* **475,** 316–323 (2011).
5. Krüger, M. & Linke, W. A. Titin-based mechanical signalling in normal and failing myocardium. *J. Mol. Cell. Cardiol.* **46,** 490–498 (2009).
6. Birukov, K. G. Small GTPases in mechanosensitive regulation of endothelial barrier. *Microvasc. Res.* **77,** 46–52 (2009).
7. Wang, N., Tytell, J. D. & Ingber, D. E. Mechanotransduction at a distance: mechanically coupling the extracellular matrix with the nucleus. *Nature Rev. Mol. Cell Biol.* **10,** 75–82 (2009).
8. Stossel, T. P. *et al.* Filamins as integrators of cell mechanics and signalling. *Nature Rev. Mol. Cell Biol.* **2,** 138–145 (2001).
9. Nakamura, F., Stossel, T. P. & Hartwig, J. H. The filamins: organizers of cell structure and function. *Cell Adh. Migr.* **5,** 160–169 (2011).
10. Ohta, Y., Hartwig, J. H. & Stossel, T. P. FilGAP, a Rho- and ROCK-regulated GAP for Rac binds filamin A to control actin remodelling. *Nature Cell Biol.* **8,** 803–814 (2006).
11. Sprague, B. L., Pego, R. L., Stavreva, D. A. & McNally, J. G. Analysis of binding reactions by fluorescence recovery after photobleaching. *Biophys. J.* **86,** 3473–3495 (2004).
12. Nakamura, F., Osborn, T. M., Hartemink, C. A., Hartwig, J. H. & Stossel, T. P. Structural basis of filamin A functions. *J. Cell Biol.* **179,** 1011–1025 (2007).
13. Wang, N., Butler, J. P. & Ingber, D. E. Mechanotransduction across the cell surface and through the cytoskeleton. *Science* **260,** 1124–1127 (1993).
14. Calderwood, D. A. *et al.* Increased filamin binding to β-integrin cytoplasmic domains inhibits cell migration. *Nature Cell Biol.* **3,** 1060–1068 (2001).
15. Lad, Y. *et al.* Structure of three tandem filamin domains reveals auto-inhibition of ligand binding. *EMBO J.* **26,** 3993–4004 (2007).
16. Heikkinen, O. K. *et al.* Atomic structures of two novel immunoglobulin-like domain pairs in the actin cross-linking protein filamin. *J. Biol. Chem.* **284,** 25450–25458 (2009).
17. Pentikäinen, U. & Ylanne, J. The regulation mechanism for the auto-inhibition of binding of human filamin A to integrin. *J. Mol. Biol.* **393,** 644–657 (2009).
18. Chen, H. S., Kolahi, K. S. & Mofrad, M. R. Phosphorylation facilitates the integrin binding of filamin under force. *Biophys. J.* **97,** 3095–3104 (2009).
19. Nakamura, F. *et al.* Molecular basis of filamin A-FilGAP interaction and its impairment in congenital disorders associated with filamin A mutations. *PLoS ONE* **4,** e4928 (2009).
20. Koenderink, G. H. *et al.* An active biopolymer network controlled by molecular motors. *Proc. Natl Acad. Sci. USA* **106,** 15192–15197 (2009).
21. Humphrey, D., Duggan, C., Saha, D., Smith, D. & Kas, J. Active fluidization of polymer networks through molecular motors. *Nature* **416,** 413–416 (2002).
22. Smith, D. M. *et al.* Molecular motor-induced instabilities and crosslinkers determine biopolymer organization. *Biophys. J.* **93,** 4445–4452 (2007).
23. Kanchanawong, P. *et al.* Nanoscale architecture of integrin-based cell adhesions. *Nature* **468,** 580–584 (2010).
24. Grashoff, C. *et al.* Measuring mechanical tension across vinculin reveals regulation of focal adhesion dynamics. *Nature* **466,** 263–266 (2010).
25. Na, S. *et al.* Rapid signal transduction in living cells is a unique feature of mechanotransduction. *Proc. Natl Acad. Sci. USA* **105,** 6626–6631 (2008).
26. Kiema, T. *et al.* The molecular basis of filamin binding to integrins and competition with talin. *Mol. Cell* **21,** 337–347 (2006).
27. Sanz-Moreno, V. *et al.* Rac activation and inactivation control plasticity of tumor cell movement. *Cell* **135,** 510–523 (2008).
28. Shifrin, Y., Arora, P. D., Ohta, Y., Calderwood, D. A. & McCulloch, C. A. The role of FilGAP-filamin A interactions in mechanoprotection. *Mol. Biol. Cell* **20,** 1269–1279 (2009).
29. Johnson, C. P., Tang, H. Y., Carag, C., Speicher, D. W. & Discher, D. E. Forced unfolding of proteins within cells. *Science* **317,** 663–666 (2007).
30. Krieger, C. C. *et al.* Cysteine shotgun-mass spectrometry (CS-MS) reveals dynamic sequence of protein structure changes within mutant and stressed cells. *Proc. Natl Acad. Sci. USA* **108,** 8269–8274 (2011).

Supplementary Information is linked to the online version of the paper at www.nature.com/nature.

Acknowledgements The authors acknowledge the Harvard Materials Research and Engineering Center (DMR-0820484) for confocal imaging, and M. Ginsberg, J. Lippincott-Schwartz and V. Verkhusha for providing complementary DNA for PA-GFP and PA-mCherry constructs. We thank T. Collins for technical assistance, L. Jawerth and V. Zaburdaev for discussions, and J. Wilking and K. Guenthner for help with the manuscript. This work was supported by grants NIH R01 HL19429 (T.P.S.) and NIH T32 HL07680 (A.J.E.) and by the Harvard University Science and Engineering Committee Seed Fund for Interdisciplinary Science (D.A.W., T.P.S., F.N.).

Author Contributions The project was initiated by T.P.S., F.N. and D.A.W. Experiments were designed by A.J.E., T.P.S., J.H.H. and F.N. Proteins and materials were synthesized and purified by F.N. and A.J.E. FLAC experiments were performed by A.J.E. and binding assays were performed by F.N. Data was analysed by A.J.E. All authors discussed data and aided in preparing the manuscript. A.J.E. and F.N. contributed equally to this project.

Author Information Reprints and permissions information is available at www.nature.com/reprints. The authors declare no competing financial interests. Readers are welcome to comment on the online version of this article at www.nature.com/nature. Correspondence and requests for materials should be addressed to F.N. (fnakamura@rics.bwh.harvard.edu) or A.J.E. (aje@seas.harvard.edu).

METHODS

Protein design and synthesis. Actin was purified from rabbit skeletal muscle and gel-filtered (HiLoad 16/60 Superdex 200pg; GE Healthcare) in G buffer[12] (2 mM Tris-HCl, 0.2 mM ATP, 0.2 mM $CaCl_2$, 0.2 mM DTT and 0.005% NaN3, pH 8.0). Aliquots of purified G-actin were frozen in liquid nitrogen and stored at −80 °C. Before use, G-actin was thawed 12 h in advance and dialyzed against fresh G buffer. Myosin II from rabbit skeletal muscle was obtained from Cytoskeleton (Denver). Human full-length FLNA and FilGAP were expressed using a baculovirus expression system (Invitrogen) in sf9 insect cells and purified as previously described[19]. All the point or deletion mutants were generated using the QuickChange site-directed mutagenesis kit (Agilent Technologies). FilGAP and integrin constructs were expressed in sf9 cells as follows. The complementary DNA (cDNA) encoding PAFPs (PA-GFP and PA-mCherry, which were kind gifts from Jennifer Lippincott-Schwartz, NIH) were amplified by PCR using the forward primer GAAGATCTATGGTGAGCAAGGGCGAGG and the reverse primer CGGGATCCCTTGTACAGCTCGTCCATG, and introduced into BamHI sites of pFASTBAC-HTb vector[12] to construct pFASTBAC-HTb-PAFPs. The cDNA encoding the cytoplasmic domain (amino acids 769–789) of human β_7-integrin was amplified by PCR using pET15-G4-integrin β_7 (a kind gift from Mark Ginsberg, UC San Diego) as a template with the forward primer GCGGATCCAA CTGGAAGCAGGACAGTAATC and the reverse primer CGGAATTCAGCG AGGATTGATGGTGG, and inserted into BamHI/EcoRI sites of pFASTBAC-HTb-PAFPs. For FilGAP, the cDNA encoding PAFPs was introduced into pFASTBAC-HTa-FilGAP at the XbaI cleavage site[19]. The expressed proteins were purified by Ni-NTA affinity and gel filtration chromatography (Superose 12 and Superdex 200, GE Healthcare) as previously described[19]. Protein concentration was measured by absorption at 280 nm using parameters calculated with ProtParam (http://au.expasy.org/tools/protparam.html). Genetic fusion of PAFPs to the binding partners[31] did not affect the binding-partner activity. Purified PAFP FilGAP proteins interact with full-length FLNA in the same dose-dependent manner as unlabelled FilGAP, and do not bind to the FLNA M2474E mutant, which lacks the FilGAP-binding site (Supplementary Fig. 2a). The PAFP-tagged cytoplasmic tail of β_7-integrin was also found to retain its binding behaviour with FLNA, and predominantly interacts with the FLNA del41 variant, where the autoinhibitory ligand-binding site is constitutively exposed[15,32] (Supplementary Fig. 2b, c).

Protein pull-down assay. The purified His-FilGAP and His-PAFP FilGAP constructs were incubated with increasing amounts of FLAG-FLNA and 20 µl of FLAG-specific mAb M2 agarose (50% (v/v) slurry, Sigma) in binding buffer (50 mM Tris-HCl, 150 mM NaCl, 0.1% (w/v) Triton X-100, 0.1 mM β-mercaptoethanol, 0.1 mM EGTA, pH 7.4; 400 µl) for 1 h at 25 °C. The beads were sedimented and washed three times with binding buffer. Proteins bound to the beads were solubilized in SDS sample buffer and separated by 9.0% (w/v) SDS–PAGE followed by immunoblotting using rabbit polyclonal antibodies (pAbs) against FilGAP[10]. For integrin, the purified His-PAFP β_7-integrin (amino acids 769–789) was incubated with increasing amounts of wild-type and mutant (del41; amino-acid residues 2126–2167 are deleted) FLAG-FLNA and 40 µl of FLAG-specific mAb M2 agarose (50% (v/v) slurry, Sigma) in binding buffer (25 mM Tris-HCl, 50 mM NaCl, 0.1% (w/v) Tween 20, 1 mM DTT, 10% sucrose, 5 mM $MgCl_2$, 1 mM EGTA, pH 7.4; 400 µl) for 2 h at 25 °C. The beads were sedimented and washed three times with the binding buffer. Proteins bound to the beads were solubilized in SDS sample buffer and separated by 10.0% (w/v) SDS–PAGE followed by immunoblotting using mouse mAb against His conjugated with horseradish peroxidase (Sigma). For the peptide pull-down assay, a synthetic peptide of the β_7-integrin cytoplasmic domain (Cys-^{771}KQDSNPLYKSAITTTINPR^{789}) was immobilized on Sulfo-Link agarose beads (1 mg ml^{-1}) and mixed with increasing amounts of wild-type and mutant (del41, AA/DK, A2272D/A2274K) FLNA. Bound FLNA was detected by immunoblotting using mouse mAb to FLNA.

Reconstitution of actin-FLNA networks. Activity buffer[10] (AB; 25 mM imidazole, 150 mM KCl, 5 mM MgATP, 0.2 mM $CaCl_2$, and 1 mM DTT, pH 7.4) and F-actin polymerization buffer[33] (FB; 20 mM Tris-HCl, 2 mM $MgCl_2$, 100 mM KCl, 0.2 mM DTT, 0.2 mM $CaCl_2$, 0.5 mM ATP, pH 7.5) were formulated as established previously. Shear cell samples consisted of 24 µM actin, 0.12 µM FLNA, ×1 FB, 2 µM Alexa 546 phalloidin and either PA-GFP FilGAP or PA-GFP β_7-integrin.

Shear-cell design and measurements. A P-780 (Physik Instrumente) piezomotor, incorporated into a home-built microscope stage, was controlled using LABVIEW software (National Instruments). The sample component of the microscope stage had as its lower plate a stationary glass coverslip within a stainless steel frame and had a glass upper plate connected by a steel post to the piezo-motor. The gap between the lower and upper plates was 300 µm. A lateral shear was applied as illustrated in Supplementary Fig. 8. Strain is defined as the change of length divided by the original length. Thus, a 300-µm vertical distance that is deformed to 312 µm when sheared laterally by 85 µm is under an engineering strain of 1.04, or 4%. The parameter γ is defined by the lateral shear divided by the sample thickness, yielding 85/300, or 0.28. Using a MATLAB-based Monte Carlo simulation of affine deformation, we calculated that a uniaxial shear strain of 0.28 causes the angle of an isotropic distribution of FLNA crosslinks initially at 90° to increase and decrease their opening angles symmetrically about 90° (on respective sides of the initially perpendicular intersection; Supplementary Fig. 8). Looking at the positive half of the distribution suggests that the weighted mean increase in opening angle is ∼6.1°, with a peak of ∼7.6°.

Myosin II system. To examine the effects of cytoskeleton-induced stress, and as a physiological technique complementary to external shear, we included 1 µM myosin II in the networks to generate contractile stress as illustrated in Supplementary Fig. 9 and Supplementary Movie 3. Individual myosin II molecules bind their tail regions together to form minifilaments, bipolar assemblies of 8–13 myosin molecules[21]. These minifilaments allow the otherwise non-processive myosin II to operate collectively with an increased duty cycle, binding the minifilaments to actin filaments long enough for filament sliding and network contraction to occur. At 150 mM KCl, approximately 8–13 myosin molecules associate into each minifilament[21]. The number of myosin minifilaments per actin filament, $N_{mf/fil}$, may be calculated from $N_{mf/fil} = [m]n_{fil}/[a]n_{mf}$, where $[m]$ is the molar concentration of myosin, n_{fil} is the number of actin monomers per actin filament, $[a]$ is the molar concentration of actin and n_{mf} is the number of myosin molecules per minifilament[22]. On the basis of an average actin filament length of ∼5 µm and there being 13 myosin molecules per minifilament, we estimate that approximately six minifilaments bind per actin filament. Repeating this estimation with FLNA instead of myosin, we estimate that there are five FLNA crosslinks per actin filament, on the basis of each crosslink being composed of two FLNA molecules. Thus, the density of myosin minifilaments per actin filament is approximately equal to that of FLNA crosslinks.

Samples were composed of 24 µM actin, 0.12 µM FLNA, 1 µM myosin II, ×1 AB and 2 mM caged ATP, along with 2 µM Alexa 546 phalloidin and 50 nM PA-GFP FilGAP or 2 µM Alexa 488 phalloidin and 50 nM PA-mCherry β_7-integrin.

Each sample was allowed to polymerize and consume available ATP over ∼6 h, at which point myosin minifilaments had ceased contracting and were in a rigor state. FLAC measurements were then performed on the ATP-free unstressed network. Subsequently, the caged ATP (Sigma) was released by a 4-s exposure to a diffuse, 50-mW, 365-nm light-emitting diode (Prizmatix). Within 3 s, the network could be seen to become active, and it substantially homogenized within approximately 5 min. FLAC measurements were repeated in the active myosin-stressed network 10–20 min after ATP release, to quantify the strain-dependent binding activity.

Imaging and analysis. Fluorescence recovery after photobleaching (FRAP) provides an effective method to measure the diffusion and binding interactions of fluorescent proteins[11]; however, the time resolution of FRAP is not adequate for fast transient events. To overcome this time limitation, we have developed FLAC, which takes advantage of the rapid photoactivation or conversion of novel PAFPs[31] (Supplementary Figs 4 and 5). In FLAC, an initially non-fluorescent sample is locally pulsed with 405-nm light, activating PAFP fluorescence, and the time-dependent decay of the PAFP intensity reveals its diffusion and binding kinetics. An additional advantage is that FLAC may present more accurate binding/diffusion information than FRAP, as adequate photobleaching requires harsh conditions[34]

Time-dependent fluorescence images were acquired with a confocal microscope (TCS SP5, Leica) using a ×10, 0.3 NA objective with images captured every 30–100 ms. PAFPs were activated using a 50-ms, ∼5-mW shuttered pulse from an external, 405-nm laser (Bestofferbuy) coupled into the confocal microscope using its non-descanned X1 port. A custom-built filter cube was installed with the filter holder rotated azimuthally by 90° to allow the 405-nm laser light entering the X1 port to be reflected upwards to the objective through a long-pass dichroic filter (Di01-R405-25x36, Semrock) and illuminate a 2-µm spot in the centre of the sample x–y plane.

Fluorescence in the photoactivation region was monitored in time and constitutes the principal data for the experiments. Data was collected before, during and after photoactivation and analysed in MATLAB. Fluorescence before activation represents the background signal, and was mainly a mixture of detection noise and background fluorescence. The background was defined as zero and subtracted from the data for each measurement. Data collected after activation was normalized to its maximum value, which was reached ∼10 ms after photoactivation. Thus, fluorescence intensity data sets range from 1 at time zero after normalization and approach zero (background) at long times. Although a wide variety of fitting algorithms and procedures exist for FRAP, which in its analysis is mathematically similar to FLAC, we use a single exponential decay, $I(t) = ae^{-t/k} + c$, to fit our data. These fits are accurate, allow us to differentiate data quantitatively as simply as possible with a single time constant, k (the characteristic fluorescence decay time),

and do not invoke a variety of free parameters or models with a-priori assumptions[11]. In each case, the fluorescence intensity decay is quantified and numerically compared using the same individual sample with and without strain to ensure consistency, eliminate artefacts or variability, and isolate mechanical strain as the single variable. In the case of single-step uniaxial strain presented in Fig. 2, data were fitted to $I(t) = ae^{-t/k} + 0.5e^{-t/(0.15s)} + c$ to provide a more accurate fit and compensate for the rapid diffusion of free fluorophore.

Photobleaching decays times were measured by photoactivating PAFP nonspecifically adsorbed to the glass surface, and were found to be in excess of 800 s, making them negligible on the timescale of FLAC experiments ($<$10 s), as shown in Supplementary Fig. 7. Photoconversion times were determined by acquiring fluorescence intensity images of PAFP adsorbed to glass every 3 ms during a 50-ms, 405-nm activation flash, as shown in Supplementary Fig. 4.

31. Fernández-Suárez, M. & Ting, A. Y. Fluorescent probes for super-resolution imaging in living cells. *Nature Rev. Mol. Cell Biol.* **9,** 929–943 (2008).
32. van der Flier, A. *et al.* Different splice variants of filamin-B affect myogenesis, subcellular distribution, and determine binding to integrin β subunits. *J. Cell Biol.* **156,** 361–376 (2002).
33. Nakamura, F., Osborn, E., Janmey, P. A. & Stossel, T. P. Comparison of filamin A-induced cross-linking and Arp2/3 complex-mediated branching on the mechanics of actin filaments. *J. Biol. Chem.* **277,** 9148–9154 (2002).
34. Weissmann, C. *et al.* Microtubule binding and trapping at the tip of neurites regulate tau motion in living neurons. *Traffic* **10,** 1655–1668 (2009).